

## Studies of the dielectric and ferroelectric properties of PZT: NZF magnetoelectric composites

Rekha Rani<sup>a,c</sup>, J.K. Juneja<sup>b</sup>, K.K. Raina<sup>c</sup> and Chandra Prakash<sup>d,\*</sup>

<sup>a</sup>Electroceramics Research Lab, GVM Girls College, Sonepat-131001, India

<sup>b</sup>Department of Physics, Hindu College, Sonepat-131001, India

<sup>c</sup>School of Physics & Material Science, Thapar University, Patiala-147004, India

<sup>d</sup>DIRECTORATE OF ER&IPR, DRDO, DRDO Bhawan, New Delhi-110105, India

**Piezoelectric-magnetostrictive (magnetoelectric) composites using piezoelectric lead zirconate titanate (PZT) ceramic and magnetostrictive Ni-Zn ferrite (NZF) with compositional formulae  $(1-x) \text{PbZr}_{0.65} \text{Ti}_{0.35} \text{O}_3 - x \text{Ni}_{0.8} \text{Zn}_{0.2} \text{Fe}_2 \text{O}_4$  with  $x = 0$  to  $0.15$  in steps of  $0.05$ , were prepared by a conventional solid state route. The presence of individual phases was confirmed using X-ray diffraction. Dielectric properties were studied as a function of temperature and frequency presuming that the interactions between the piezoelectric and magnetostrictive phases may result in various anomalies in the dielectric properties of these composites. To study the ferroelectric properties, P-E hysteresis loops were recorded.**

**Key words:** Magnetoelectric, Ferroelectric, Spinel, Perovskite, Dielectric, Dispersion.

### Introduction

In recent years, magnetoelectric (ME) materials with a coexistence of both ferroelectric and ferromagnetic ordering simultaneously have been drawn increasing interest due to many technological applications such as sensors for magnetic field measurements, transducers for magnetoelectric conversion and magnetoelectric memory devices [1-4] etc. These magnetoelectric materials are classified into two groups, single phase and composites. There are very few single-phase magnetoelectric materials which do not have any technological applications due to a small ME voltage coefficient and temperature constraints [5-8]. A composite of piezoelectric-magnetostrictive phases is expected to show a large ME voltage coefficient resulting from magnetostriction-induced deformation and the generation of a piezoelectric charge [9-12]. All the properties of these composites are classified as sum, combination and product properties. The product property of such composites i.e. a strain induced ME effect is of technical importance for multifunctional devices. Further, the sum properties of these composites such as the dielectric constant, density etc. and properties of individual phases such as ferroelectric P-E hysteresis loops due to the presence of the ferroelectric phase (PZT) and ferromagnetic M-H hysteresis loops due to the presence of a ferrite phase (NZF) are also equally important as they affect the product property. The most widely studied systems that have been reported correspond

to composites of  $\text{NiFe}_2\text{O}_4$ ,  $\text{CoFe}_2\text{O}_4$ ,  $\text{MnFe}_2\text{O}_4$ ,  $\text{ZnFe}_2\text{O}_4$ , terfenol ferrites with PZT, PMN-PT, PVDF and  $\text{BaTiO}_3$  [13-16]. The present study is concerned with the synthesis of bulk PZT : Ni-Zn ferrite composites and studies of the dielectric and ferroelectric properties of these composites. A  $\text{PbZr}_{0.65} \text{Ti}_{0.35} \text{O}_3$  (PZT) composition for the ferroelectric phase was selected because of its lower sintering temperature, stronger dielectric and piezoelectric properties and higher resistivity [17] as compared to other ferroelectrics and a Zn doped nickel ferrite as the ferrite phase was selected due to its high resistivity, high piezomagnetic coefficient [18] and because it is very stable in the PZT matrix [19].

### Experimental

Individual phases (ferroelectric and ferrite) were prepared by a conventional solid state reaction route. AR grade  $\text{PbO}$ ,  $\text{ZrO}_2$  and  $\text{TiO}_2$  for the ferroelectric phase were weighed in the required molar proportions. An excess of 2% of  $\text{PbO}$  was added to compensate for lead loss during sintering. The mixing process was carried out by ball milling in distilled water using zirconia balls as the milling media. The dried powder was calcined at  $800^\circ\text{C}$  for 4 h. After ball milling, the powder mixture was re-calcined at  $1000^\circ\text{C}$  for 4 h. AR grade  $\text{NiO}$ ,  $\text{ZnO}$  and  $\text{Fe}_2\text{O}_3$  were used as raw materials for synthesis of the ferrite phase. The powder mixture was ball milled and then calcined at  $1000^\circ\text{C}$  for 4 h. A small amount of  $\text{MnO}_2$  (0.5% by weight) was added to increase the resistivity of the ferrite phase. The powder mixture was ball milled again and then re-calcined at  $1100^\circ\text{C}$  for 4 h. The composites with compositional formula  $(1-x) \text{PbZr}_{0.65} \text{Ti}_{0.35} \text{O}_3 - x \text{Ni}_{0.8} \text{Zn}_{0.2} \text{Fe}_2 \text{O}_4$

\*Corresponding author:

Tel : +91-11-2300-7350

Fax: +91-11-2301-7582

E-mail: cprakash@hqr.drdo.in

( $x = 0$  to  $0.15$  in steps of  $0.05$ ) were prepared by mixing the two phases. The mixing process was carried out by ball milling in distilled water. After drying, a small amount of diluted polyvinyl alcohol (2-3 drops) was added to the powder mixture as a binder which was pressed into circular discs of  $1\text{mm}$  thickness and  $15\text{ mm}$  diameter using a uniaxial hydraulic press. The pellets were finally sintered at  $1200\text{ }^{\circ}\text{C}$  for  $4\text{ h}$  with a heating rate of  $5\text{ }^{\circ}\text{C}\cdot\text{minute}^{-1}$  in a micro-processor controlled furnace. The experimental density of sintered pellets was determined using Archimedes principle. X-ray diffraction (XRD) patterns were recorded using a Philips XPERT-PRO Diffractogram with a  $\text{CuK}_{\alpha}$  ( $\lambda = 1.5406\text{ \AA}$ ) source operated at  $45\text{ kV}/40\text{ mA}$ . To measure the dielectric and ferroelectric properties, the sintered pellets were ground and then electrodeed properly using silver paste on flat surfaces by heating at  $400\text{ }^{\circ}\text{C}$  for  $30\text{ minutes}$  to ensure good ohmic contacts. The dielectric properties as a function of frequency (100 Hz-1 MHz) at room temperature and temperature ( $35\text{-}500\text{ }^{\circ}\text{C}$ ) at  $1\text{ kHz}$ ,  $10\text{ kHz}$  and  $100\text{ kHz}$  were measured using an Agilent 4284A LCR meter. P-E hysteresis loops were recorded at  $20\text{ Hz}$  using an automated P-E loop tracer based on a Sawyer-Tower circuit.

## Results and Discussion

Fig. 1 shows the XRD patterns for individual phases (PZT & NZF) and composite samples with  $x = 0.05$ ,  $0.10$  and  $0.15$ . The patterns for composite samples show well-defined peaks with specific indices characteristic of perovskite and spinel structures. This confirms the perovskite structure in the ferroelectric phase (PZT) and the cubic spinel structure in the ferrite phase (NZF). No extra peaks were observed which confirms that no chemical reaction took place between the two phases. Comparison of XRD patterns shows that there is an increase in the intensity

**Table 1.** Variation of relative density,  $T_c$ ,  $\epsilon_{RT}$ ,  $\epsilon_{max}$ ,  $\tan\delta_{RT}$  and  $\tan\delta_{max}$  for different values of  $x$  at  $100\text{ kHz}$

x	Relative Density	$T_c(^{\circ}\text{C})$	$\epsilon_{RT}$	$\epsilon_{max}$	$\tan\delta_{RT}$	$\tan\delta_{max}$
0	94.51	422	822	19586	0.023	0.101
0.05	92.65	394	626	10761	0.025	0.151
0.10	88.77	408	591	7636	0.034	0.216
0.15	88.98	407	405	5276	0.116	0.306

and number of peaks corresponding to the ferrite phase for  $x = 0.15$  due to the higher concentration of ferrite. The relative density for all the samples was calculated and is given in Table 1. Comparison shows that there is a decrease in density with an increase in the ferrite content ( $x$ ) and this is due to the low density of NZF ferrite as compared to PZT. However, the composite with  $x = 0.15$  has a slightly higher density and that may be due to better compaction and sinterability [19].

Fig. 2 shows the variation of dielectric constant with temperature for all the compositions at three different frequencies ( $1\text{ kHz}$ ,  $10\text{ kHz}$  and  $100\text{ kHz}$ ). From these graphs, we observe that initially the dielectric constant increases with an increase in temperature and attains a maximum value at the ferroelectric Curie temperature ( $T_c$ ) followed by a decrease in the dielectric constant with a further increase in the temperature for all values of  $x$ . From the dielectric versus temperature curve for  $x = 0$ , a dielectric dispersion is observed near and above  $T_c$ , while for  $x = 0.05$ ,  $0.10$  &  $0.15$ , a dielectric dispersion is clearly observed over a wide range of temperature around  $T_c$ . Also, the dielectric peaks get broadened and suppressed with an increase in  $x$ . This is due to the microstructural inhomogeneity created with an increase in  $x$  [20].

In the paraelectric region, it is observed that there is an increase in the dielectric constant with increase in the temperature for  $x = 0.10$  &  $0.15$  and this increase is more pronounced for  $x = 0.15$ . But with an increase in the measurement frequency this observed behavior gradually reduces showing that it could be related to a low frequency relaxation process [21]. This increase in dielectric constant at high temperatures is due to an increase in the dielectric polarization which is a result of thermally-activated electron hopping between  $\text{Fe}^{+2} \leftrightarrow \text{Fe}^{+3}$  ions as well as  $\text{Ni}^{+2} \leftrightarrow \text{Ni}^{+3}$  ions present in the ferrite phase. Fig. 3 shows the temperature dependence of the dielectric constant and loss tangent at  $100\text{ kHz}$  for all the samples. The higher values of the loss tangent at high temperatures are attributed to the thermal conductivity losses and similar behavior has been reported by other workers [22, 23]. The values of ferroelectric Curie temperature ( $T_c$ ), room temperature dielectric constant ( $\epsilon_{RT}$ ), room temperature loss tangent ( $\tan\delta_{RT}$ ), dielectric constant at  $T_c$  ( $\epsilon_{max}$ ) and loss tangent at  $T_c$  ( $\tan\delta_{max}$ ) at  $100\text{ kHz}$  for all the samples are given in Table 1. There is a decrease in the dielectric constant and

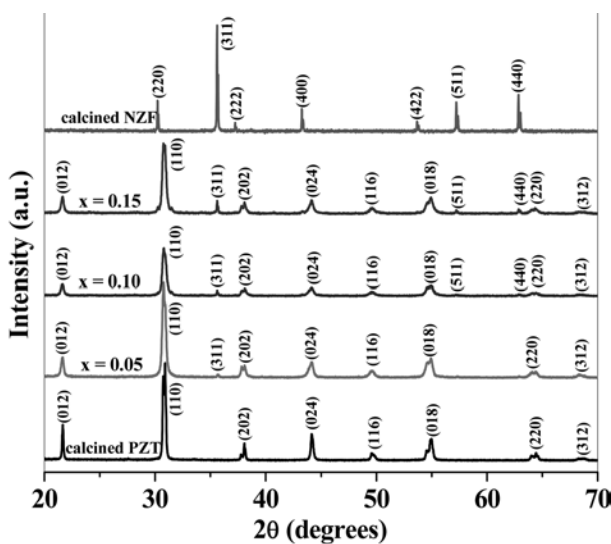


**Fig. 1.** X-Ray diffraction patterns for calcined PZT, NZF and composites.

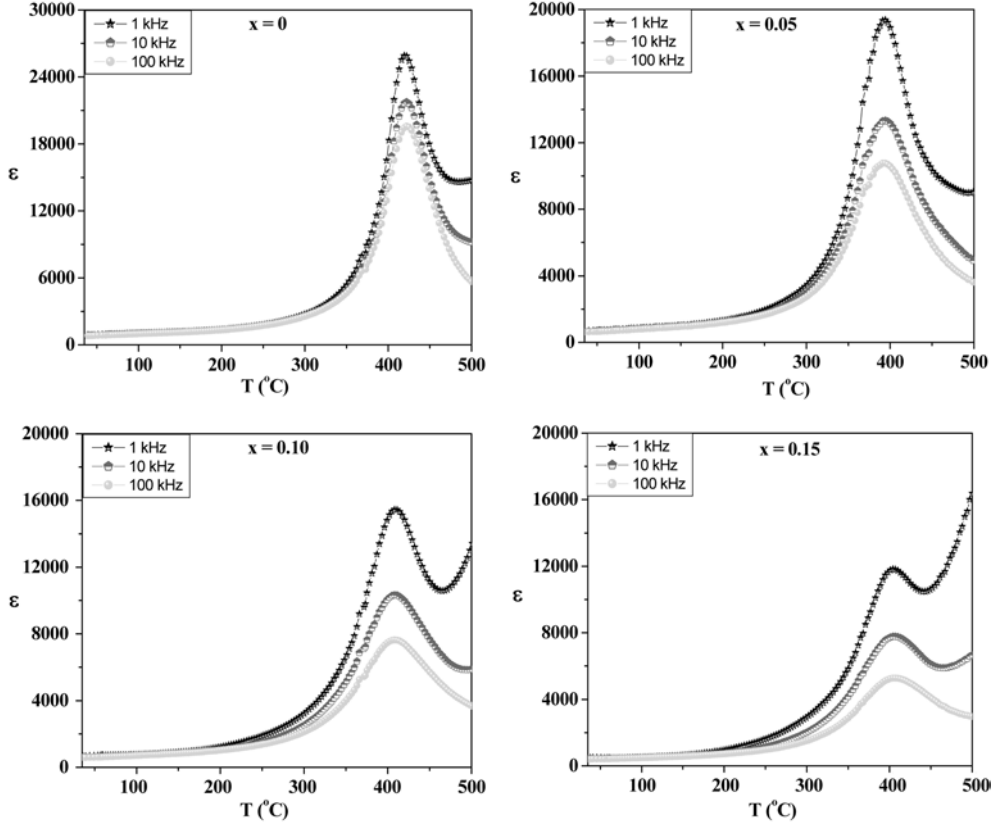


Fig. 2. Variation of the dielectric constant with temperature for all values of  $x$  at 1 kHz, 10 kHz and 100 kHz.

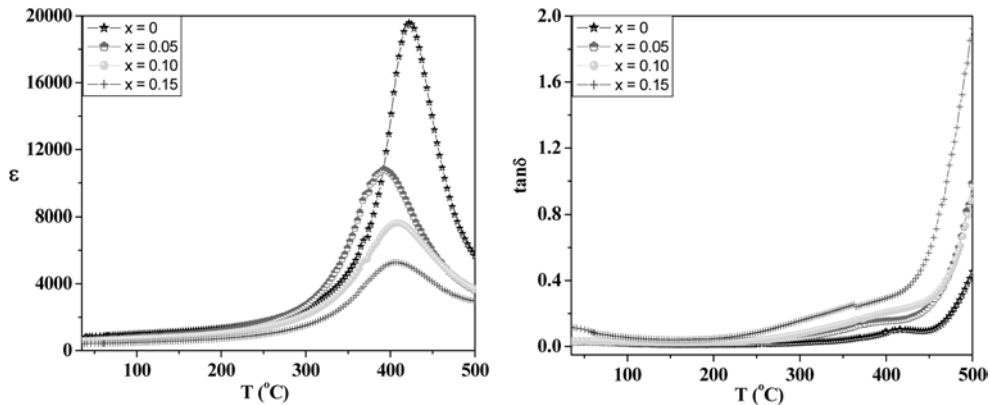


Fig. 3. Variation of the dielectric constant and the tangent loss with temperature at 100 kHz.

an increase in the loss tangent with an increase in the ferrite concentration and is already reported by many researchers [24, 25].

The variation of the dielectric constant and loss tangent with frequency at room temperature was also studied for all the samples and is shown in Fig. 4. The high values of the dielectric constant are observed at lower frequencies and this may be the result of space charge polarization due to inhomogeneity in the structure [26]. However, in the case of the composites, the high value of the dielectric constant can be explained on the basis of the fact that ferroelectric regions are surrounded by non- ferroelectric

regions similar to that in relaxor ferroelectrics [27]. The dielectric constant decreases with an increase in the frequency and this decrease is rapid for the lower frequency region because as the frequency increases, ionic and orientation polarizations decrease. A similar dispersion to that of the dielectric constant is observed in the case of the loss tangent with frequency.

Fig. 5 shows room temperature P-E hysteresis plots for  $x = 0, 0.05 \& 0.10$ . A comparison of P-E loops reveals that both the remanent polarization ( $P_r$ ) and saturation polarization ( $P_s$ ) decrease with an increase in the value of  $x$  i.e. ferroelectric behavior is weakening with an

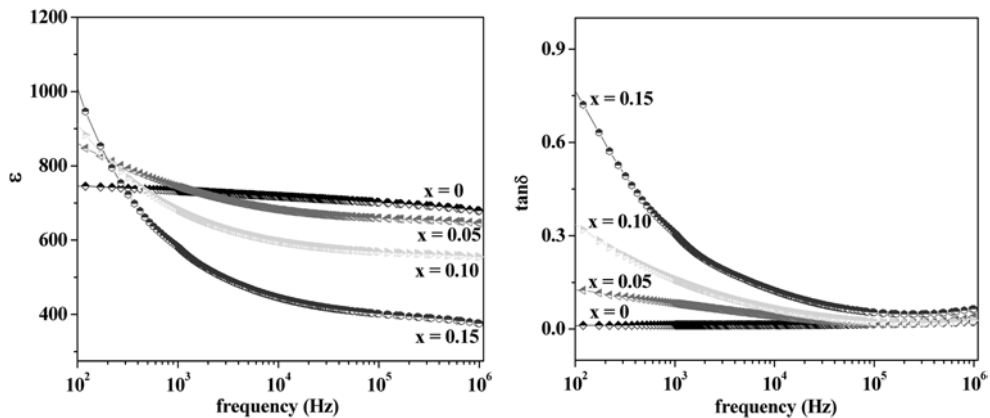


Fig. 4. Variation of the dielectric constant and the tangent loss with frequency for all values of x.

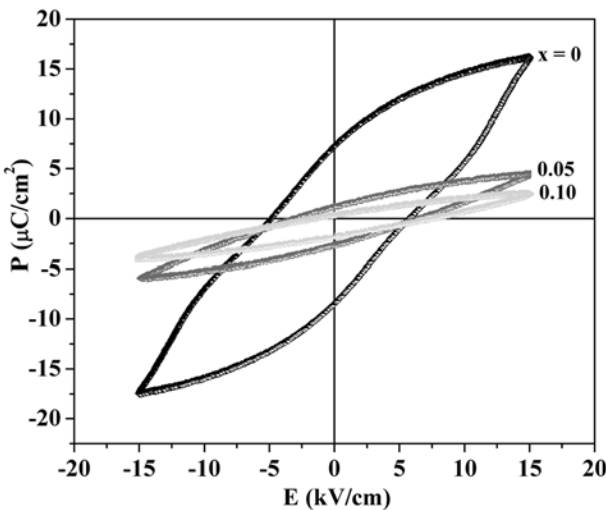


Fig. 5. Ferroelectric hysteresis loops for  $x = 0, 0.05 \& 0.10$ .

Table 2. Variation of  $P_r$ ,  $P_s$  and  $P_r/P_s$  for different values of x in  $(1-x) \text{ PbZr}_{0.65} \text{Ti}_{0.35} \text{O}_3-x \text{ Ni}_{0.8} \text{Zn}_{0.2} \text{Fe}_2\text{O}_4$ .

X	$P_r$ ( $\mu\text{C}/\text{cm}^2$ )	$P_s$ ( $\mu\text{C}/\text{cm}^2$ )	$P_r/P_s$
0	7.88	16.93	0.465
0.05	1.87	5.29	0.353
0.10	1.10	3.36	0.327

increase in the ferrite content. This may be due to a low internal polarizability [28] i.e. a decrease in the long range ordered behavior of electric dipoles because ferrite particles with a spinel structure are incorporated into the ferroelectric phase. There is not much effect on the coercive field ( $E_c$ ) by the addition of ferrite content. From Table 2, it can be seen that there is a decrease in the squareness ratio with an increase in the ferrite content which indicates a decrease in the homogeneity and uniformity of grains [29] by the addition of nickel zinc ferrite. The values of  $P_r$ ,  $P_s$  and  $P_r/P_s$  obey the rule of mixtures and go on decreasing by decreasing the concentration of the ferroelectric phase.

## Conclusions

X-ray diffraction analysis confirms the coexistence of both phases in the composite samples. There is a decrease in the dielectric constant values and an increase in the tangent loss with an increase in the ferrite content. All the samples show well-defined ferroelectric behavior.

## Acknowledgement

One of the authors (Rekha Rani) would like to thank Department of Science & Technology for awarding INSPIRE fellowship to her.

## References

- R.S. Devan, S.A. Lokare, D.R. Patil, S.S. Chougule, Y.D. Kolekar and B.K. Chougule, *J. Phys. Chem. Sol.* 67 (2006) 1524-1530.
- C.W. Nan, *Phys. Rev. B* 50 (1994) 6082-6088.
- T.H.O' Dell, *Electron. Power* 11 (1965) 266-267.
- L.P.M. Bracke and R.G. Van Vliet, *Int. J. Electron.* 51 (1981) 255-262.
- T. Lottermoser and M. Fiebig, *Phys. Rev. B* 70 (2004) 220407-220410.
- J. Wang, J.B. Neaton and H. Zheng, *Science* 299 (2003) 1719-1722.
- J. Ryu, A.V. Carazo, K. Uchino and H.E. Kim, *Jpn. J. Appl. Phys.* 40 (2001) 4948-4951.
- D.N. Astrov, *Sov. Phys. JETP* 13 (1961) 729-733.
- S.X. Dong, J.F. Li and D. Veihland, *J. Appl. Phys.* 95 (2004) 2625-2630.
- J. Van Suchetlen, *Philips Res. Rep.* 27 (1972) 28-37.
- J. Van den Boomgaard and R.A.J. Born, *J. Mater. Sci.* 13 (1978) 1538-1548.
- G. Harshe, J.P. Dougherty and R.E. Newnham, *Int. J. Appl. Electromag. Mater.* 4 (1993) 161-171.
- K. Uchino, *Ferroelectric devices*, New York, Marcel Dekker, Inc. (2000).
- R.M. Hornreich and S. Shtrikman, *Phys. Rev.* 161 (1967) 506-512.
- T.G. Lupeiko, I.V. Lisnevskaya and B.I. Zvyagintsev, *Inorg. Mater.* 31 (1995) 1139-1142.
- S. Priya and D.J. Inman, *Energy Harvesting Technologies*,

- LLC (2009).
17. S. Dutta, R.N.P. Choudhary and P.K. Sinha, Ceram. Int. 33 (2007) 13-20.
  18. R.U. Mangalraja, S. Ananthakumar, P. Manohar and F.D. Jananam, J. Magn. Magn. Mater. 253 (2002) 56-64.
  19. W.E. Kramer, R.H. Hopkins and M.R. Daniel, J. Mater. Sci. Lett. 12 (1977) 409-413.
  20. K.K. Patankar, V.L. Mathe, A.N. Patil, Y.D. Kolekar and P.B. Joshi, J. Electroceram. 6 (2001) 115-122.
  21. A.P. Barranco, J.D.S. Guerra, R.L. Noda and E.B. Araujo, J. Phys. D: Appl. Phys. 41 (2008) 215503-215507.
  22. E. Stern and A. Lurie, Phys. Rev. 123 (1981) 117-123.
  23. J. Palestro, G. Grange, R. Goutte and L. Fyrand, J. Phys. D: 7 (1974) 78-81.
  24. S. Upadhyay, D. Kumar and O. Prakash, Bull. Mater. Sci. 19 (1996) 513-525.
  25. S.L. Kadam, C.M. Kanamadi, K.K. Patankar and B.K. Chougule, Mater. Lett. 59 (2005) 215-219.
  26. K.K. Patankar, S.S. Joshi and B.K. Chougule, Phys. Lett. A 346 (2005) 337-341.
  27. D.C. Agrawal, Asian J. Phys. 6 (1997) 108.
  28. K. Carl and K.H. Hardtl, Ferroelectrics 17 (1978) 473-486.
  29. A.S. Fawzi, A.D. Sheikh and V.L. Mathe, Phys. B 405 (2010) 340-344.
  30. J. Zhai, N. Cai, Z. Shi, Y. Lin and C.W. Nan, J. Phys. D: Appl. Phys. 37 (2004) 823-827.